J Braz. Soc. Mech. Sci. Eng. (2016) 38:1199–1206
DOI 10.1007/s40430-015-0422-5

TECHNICAL PAPER

Thermal analysis of laser beam welding of nickel-based super alloy Inconel 625 to AISI 316L, using Gaussian optics theory in keyhole

Ahmad Nejad Ebrahimi[1] · N. Bani Mostafa Arab[1] · M. Hoseinpour Gollo[1]

Received: 16 May 2015 / Accepted: 26 August 2015 / Published online: 1 October 2015

Abstract Keyhole laser welding is widely used as an industrial joining method in recent years, but it is not quantitatively understood due to its high complexity. This paper aims to provide a computational platform to quantitatively predict the thermal history of various locations such as HAZ and WM in the welded parts. The model characterizes the absorbed laser power in the keyhole wall at different depths by applying emission theory of light. Bremsstrahlung reflection, Fresnel absorption coefficient and multiple reflection, obtained from a volumetric heat flux distribution, are used to calculate using the absorbed laser beam density in the butt joint of nickel-based super alloy Inconel 625 to AISI 316L. The simulation results show that the model predicts the thermal history in various locations in good agreement with experimental results. The presented model provides a volumetric model to simulate the heat flux profile using various Fresnel absorption coefficients over the sample depth that captures the actual operation conditions.

Keywords Laser welding · Multiple reflections · Inverse Bremsstrahlung coefficient · Fresnel absorption · Gaussian optics theory

Technical Editor: Alexandre Mendes Abrao.

✉ Ahmad Nejad Ebrahimi
ahmad.ebrahimy@gmail.com

[1] Department of Mechanical Engineering, Shahid Rajaee Teacher Training University (SRTTU), Lavizan, Tehran, Iran

1 Introduction

Inconel alloy 625 is an approved material of construction under the Boiler and Pressure Vessel Code of the American Society of Mechanical Engineers (ASME), due to its good mechanical and chemical properties (e.g., corrosion resistance and retention of hardness) in elevated temperatures. It is widely used to construct the equipment for the power and nuclear industries, such as boilers and nuclear reactors [1–3]. Many pieces of these equipments need to have creep and corrosion resistance; therefore, Inconel 625 should be jointed to stainless steels (e.g., Austenitic stainless steel 316) that has high corrosion strength. However, these types of joints are highly sensitive due to the very low weldability of Inconel alloy [4–6] and therefore the welding method should be associated with minimal distortion and microstructure changes. ND:YAG laser welding process with high penetration depth and very narrow heat-affected zone is one of the fusion welding methods that can be used in highly sensitive joints. The pressure, created by the intense vaporization, tends to dig into the molten metal zone and then the laser beam penetrates deeper into the matter creating a thin hole (called keyhole) in the supplied zone [7]. In keyhole laser welding, very strong density of power is delivered to the metal that immediately evaporates surface after reaching the laser beam on the surface of the work. This phenomenon allows deep welding during ND:YAG continuous wave welding process and without any major problem, the keyhole shape is close to an inclined conical form [8, 9]. Laser beam energy is not completely absorbed to the keyhole wall, so some of it will be reflected from the work surface that some of the reflected beams can be absorbed into the keyhole wall at subsequent encounters while some of them can be reflected back [10]. This process is continued until the power of the reflected

Table 1 Chemical composition of Inconel 625

Ni	Cr	Fe	Mo	Nb + Ta	C	Mn	Si	Al	Ti
Min 58.0	20.0–23.0	Max 5.0	8.0–10.0	3.15–4.15	Max 0.10	Max 0.50	Max 0.50	Max 0.40	Max 0.40

Table 2 Chemical composition of stainless steel 316 l

C	Si	Mn	Mo	S	P	Ni	Cr	Cu	N
Max 0.03	Max 1.00	Max 2.00	2.00–3.00	Max 0.030	Max 0.045	00–15.00	16.00–18.00	–	–

beams is reduced to the extent that does not have the necessary power to influence the keyhole. The created keyhole is dependent on many factors, including welding speed (low welding speed creates a keyhole closer to the axisymmetric form and under the high speed the shape and bending of keyhole becomes more elongated) [11, 12]. Modifying the shape of the keyhole with multiple reflections improves the efficiency of the process. Due to the optical nature of the laser beam, its energy will not be completely absorbed by the surface of the work so some of it, will be reflected from the surface that the amount of reflected energy is a function of many properties of the process including shielding gas, laser frequency, temperature and the angular frequency of the laser radiation. The laser beam welding process has been studied by many; for example, Volpp and Vollertsen (2013) used an analytical modeling approach, including multiple reflections to analyze the influence of different laser intensity distributions on keyhole geometry [12]. Devendr and Ramkumar (2014) investigated the influence of filler metals and welding techniques on the structure–property relationships of Inconel 718 and AISI 316L dissimilar weldments. They articulated the effects of filler metals on the structure–property relationships to the weldments [13]. To study the formation and expansion of the keyhole, great deal of research has been done. Kaplan (1994) based on the energy balance at the keyhole wall predicted the axisymmetric form for the keyhole that predicates weld geometry at high welding speeds regardless of the fluid flow inside it [14]. Dowden et al. (1989) applied Fresnel absorption coefficient for a single uniformly linear laser source [15]. Solana and Ngero (1997) applied an axisymmetric Gaussian model for distribution of laser heat flux density in the keyhole depth of the uniform laser beam to analyze the keyhole [16]. Bachmanna et al. (2014) did an experimental and numerical investigation of an electromagnetic weld pool control for laser beam welding. Their results revealed that oscillating and steady magnetic fields can have a significant positive effect on the quality and the stability of high-power laser beam welding processes of aluminum alloys and stainless steel [17]. The motivation of this study is to develop a comprehensive volumetric heat flux model in the keyhole laser welding, So that the absorption coefficient of the laser power in the keyhole wall, varies with distance from the surface of work due to reflecting of the laser beam from the keyhole wall, and absorbing laser power due to multiple reflections of the laser beam.

2 Experimental procedure

Commercially available Inconel 625 and AISI 316L were used in this study. The dimensions of these plates were 100 × 30 × 1 mm. The chemical compositions of the base metals are listed in Tables 1 and 2. Experiments were carried out with a CW–Nd:YAG Laser, with a maximum power of 4 kW. The laser beam was delivered through a 400 mm optical fiber. The laser beam operates on a Gaussian mode ($K > 0.9$) at a wavelength of 10.9 μm. Metallographic and SEM images were taken and copper sulfate resolved in hydrochloric acid used for etching of welded materials.

3 Finite element model

The standard finite element software ABAQUS/CAE was employed for simulating the temperature distribution in the base metals during the pulsed Nd:YAG laser welding process. One of the special features of this software is the ability to consider the temperature-dependent material properties for the workpiece. Consequently, the temperature dependency of workpiece material properties was taken into account in the simulation stage. This consideration increases the compatibility of predicted values with the experimental observation. The latent heat of melting, considered as one of the major features of the workpiece, was considered in the numerical analysis due to the crucial effect on the result of the simulation. However, when the applied heat flux is based on the specific absorption coefficients in each material, the created keyhole will be closer to the true state. In this paper to define the heat flux distribution, we used the Goldak's double ellipsoid with such constant parameters that converts this model into the parabolic shape with constant parameters and welding simulation conditions that is measured experimentally in welding speed 10 mm/s (as shown in Table 3). The numerical analyses were performed using a 10-node quadratic heat transfer tetrahedron (DC3D10)

Table 3 Finite element simulation condition and constant parameter measured experimentally

a	b	C_r	C_f	Laser power	Welding speed
0.3 mm	1 mm	0.5 mm	0.5 mm	3.5 kW	10 mm/s

mesh with the global size of 13 Rm. Approximately 95,000 elements have been generated in the sample. One of the most important factors for determining the final microstructure of welded material is the thermal history of the material.

3.1 Computation of theoretical laser beam efficiencies using energy balancing

The formation of keyhole is an important factor that affects the efficiency of the laser beam welding. The keyhole will be formed after overcoming a threshold level (r_s) that it can be defined as function of material vaporization temperature (T_V), the thermal conductivity (K), and the absorptivity at normal incidence (A), as follows:

$$r_s \propto \frac{T_V K}{A}. \tag{1}$$

As shown in the schematic diagram in Fig. 1 for steady state, before the laser beam reaches for the keyhole wall, it would have lost some of its energy due to absorption by a plasma plume (P_{plume}), and part of laser power will be lost due to reflection from the material surface P_{ref}, and therefore the laser beam power can be defined by the following formula:

$$P_{\text{effected power}} = P - P_{ref} - P_{plume}. \tag{2}$$

If the shielding gas was properly used, the absorbed laser beam power can be minimized while the laser beam gets through the keyhole wall, even though some of it can be partially absorbed (first Fresnel absorption). The percentage of the absorbed power depends on the wall angle and material's physical properties. The reflected intensity

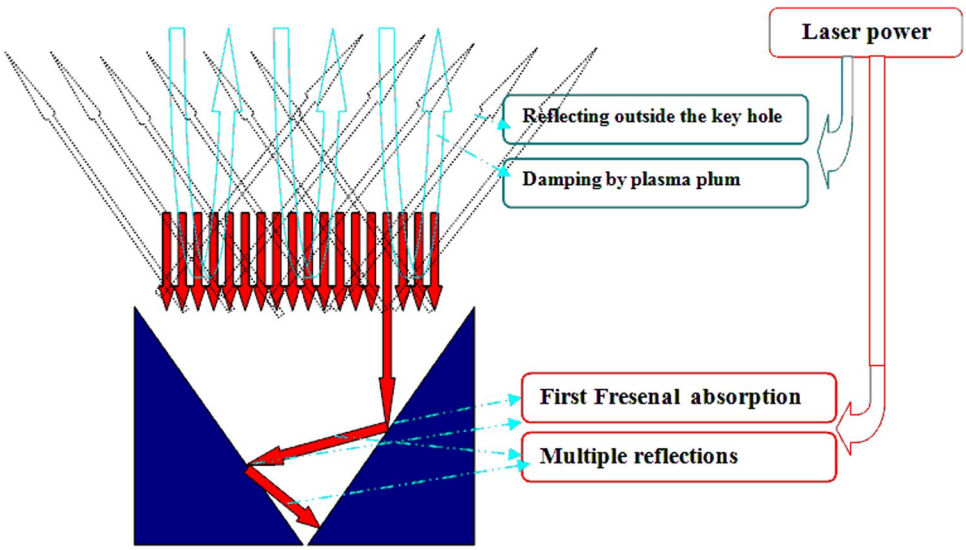

Fig. 1 Schematic diagrams showing the power balancing during keyhole laser welding

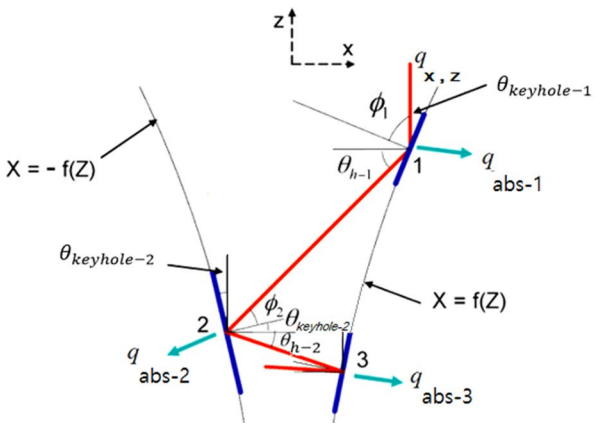

Fig. 2 Geometrical analysis for multiple reflections inside the keyhole

$$\theta_{keyhole} = \tan^{-1}\frac{dx}{dz}$$

$$\emptyset_1 = \frac{\pi}{2} - \theta_{keyhole-1}$$

$$\emptyset_{h-1} = \emptyset_1 - \theta_{keyhole-1}$$

$$\emptyset_2 = \theta_{h-1} - \theta_{keyhole-2}$$

$$\alpha_{Fresenal} = f(\emptyset)$$

will pass through the multiple reflections inside the keyhole, and between each reflection the laser ray will lose some of its intensity due to plasma absorption. The laser ray finally leaves the keyhole from the top in the case of blind key holes, or from both bottom and top in open keyholes [18]. The coupling efficiency (η_A) is defined as the portion of the laser power available for the material and is equal to the ratio of the absorbed power (P_{abs}) by the keyhole wall and the total laser power (P) [19]:

$$\eta_A = \frac{P_{abs}}{P}. \tag{3}$$

4 Results and discussion

In this paper, the thermal histories of materials have been determined at several critical points, such as weld line, HAZ and base metal using the laser power of 500 W in each material. Comparison between experimental and finite element results (Figs. 3, 4) shows that in each material "Superalloy Inconel 625 and AISI 316L", experimental results are much close to finite element results. Since there is a different laser power absorption coefficient for each material, the created keyhole in each base material is unique. Considering the variation in the absorption coefficients of different materials provide better prediction for the actual case using finite element results.

4.1 Calculation of the Fresnel absorption coefficient

The laser beam can be reflected or absorbed from the keyhole wall. At the liquid–vapor interface the angle of incidence of the laser beam is assumed to be equal to the angle of reflection. The absorption coefficient of the laser ray $\alpha_{(Fresnel)}$ can be calculated using the Fresnel formula for circular or randomly polarized light as follows:

$$\alpha_{(Fresnel)} = 1 - \frac{1}{2}\left(\frac{1+(1-\varepsilon\cos\phi)^2}{1+(1+\varepsilon\cos\phi)^2} + \frac{\varepsilon^2 - 2\varepsilon\cos\phi + 2\cos^2\phi}{\varepsilon^2 + 2\varepsilon\cos\phi + 2\cos^2\phi}\right), \tag{4}$$

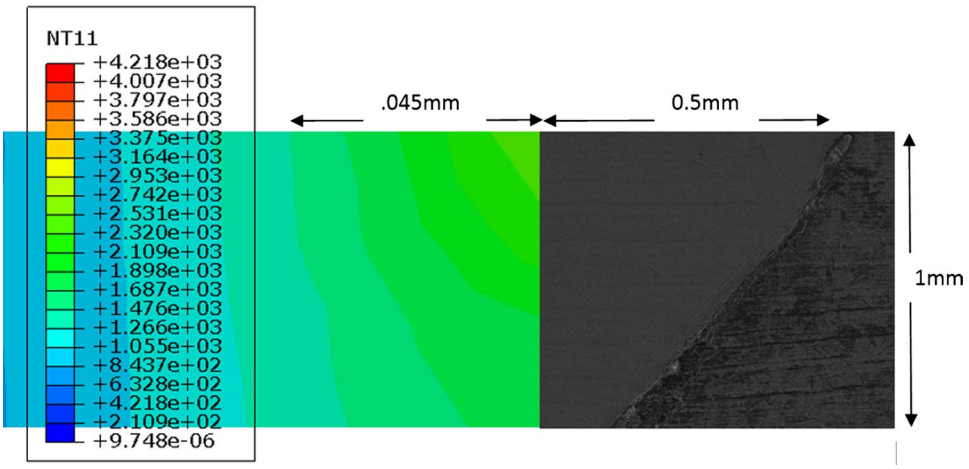

Fig. 3 Comparison of the temperature distribution by the finite element model and experimental results in Inconel 625

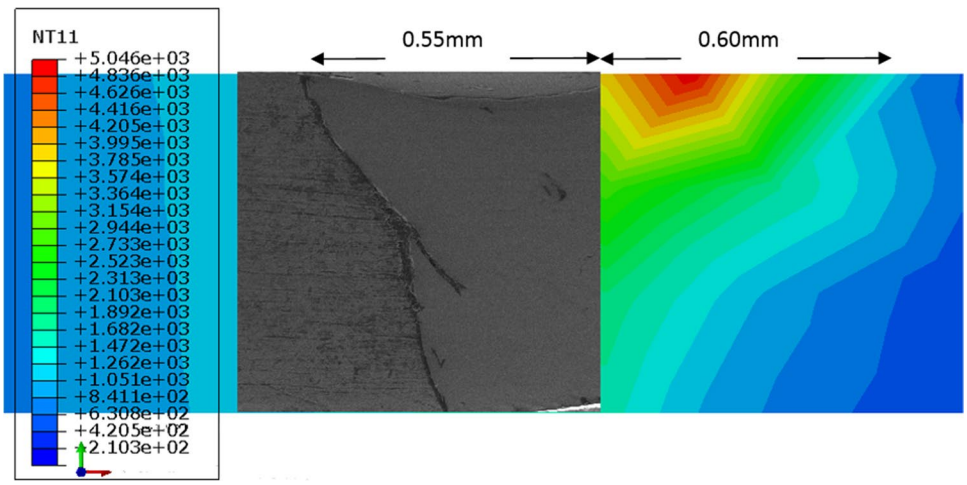

Fig. 4 Comparison of the temperature distribution by the finite element model and experimental results in stainless steel 304L

where ϕ is the angle of incidence and ε is the material-dependent constant in the Nd:YAG laser. Based on the experimental examination, the Fresnel absorption coefficient $\alpha_{(\text{Fresnet})}$ will be in the range of 4–6 %. However, this range can be changed based on material types. In this paper, a variable absorption coefficient that varies by distance from the surface has been used. For this reason, an angle of keyhole wall, perpendicular to the horizon is determined based on the equations defined in the Fig. 2. With this calculation, the keyhole wall will be defined as a cone. All of the following items using a FORTRAN subroutine have been given to ABAQUS in a transient thermal analysis; therefore, the amount of absorbed laser power can be expressed as follows:

$$p_{\text{abs}} = p\alpha_{(\text{Fresnel})} - \alpha_{\text{IB}}p, \tag{5}$$

where p is the laser power. The plasma absorption appears in the keyhole-mode laser welding that affects the characteristics of the keyhole by producing a wider or less penetrated keyhole [20]. The absorbed intensity in the keyhole by the inverse Bremsstrahlung action will be deposited back to the keyhole wall by radiation [21]. The plasma absorption coefficient is proportional to the square of the wavelength [18]. Since the wavelength of a CO_2 laser is 10.6 and 1.06 μm for Nd:YAG, Kaplan [22] reported that the plasma plume absorption outside the keyhole is approximately 1 % of the incident laser power for CO_2 lasers. Therefore, the plasma plume (outside the keyhole) can be neglected because of the shorter wavelength of the Nd:YAG laser, whereas the plasma absorption between the multiple reflections inside the keyhole was calculated.

4.2 Calculation of plasma effect

Inverse Bremsstrahlung coefficient, the most important coefficient in the absorption of laser energy into plasma, is expressed as follows:

$$\alpha_{\text{IB}} = \frac{n_e^2 e^6}{6\sqrt{3}\mu\varepsilon_0^3 ch\omega^3 m_e^2}\left[\frac{m_e}{2\pi kT_e}\right]^{0.5} g \tag{6}$$

$$g = \frac{\sqrt{3}}{\pi}\ln\left[\left(\frac{2}{\gamma_g}\right)^{\frac{5}{2}}\left(\frac{kT_e}{m_e}\right)\left(\frac{4\pi\varepsilon_0 m_e}{e^2\omega}\right)\right], \tag{7}$$

where n_e is the electron density, m_e electron mass, T_e effective temperature, ε_0 vacuum permittivity constant, γ_g a fixed quantity that is approximately equal to 1.78 and ω angular frequency of the laser radiation.

The amount of power that is absorbed by the plasma column using the inverse Bremsstrahlung coefficient is equal to:

$$P_{\text{plume}} = \alpha_{\text{IB}}p. \tag{8}$$

4.3 Multiple reflections of the laser beam in the keyhole

The keyhole profile can be calculated by considering only the first Fresnel absorption; the keyhole profile was converted to polynomial equation using the least squares method that can be used to calculate the Fresnel absorption coefficient at any location. Between two reflections, the laser beam loses intensity due to the plasma absorption. Geometry calculation and density of Fresnel absorption coefficient are considered in Kaplan's analysis [24].

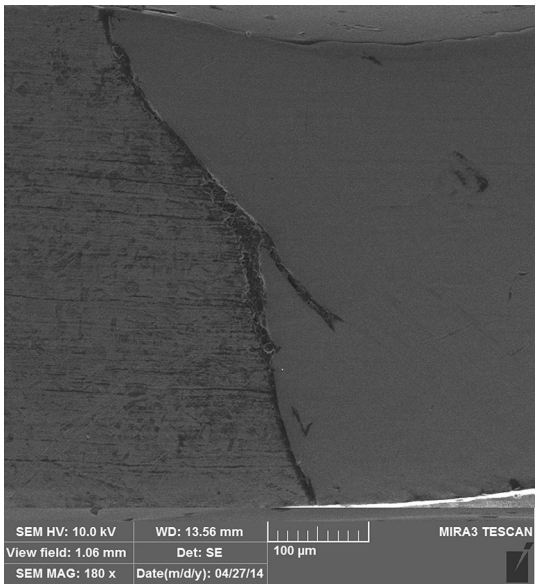

Fig. 5 Keyhole profile in stainless steel 304L

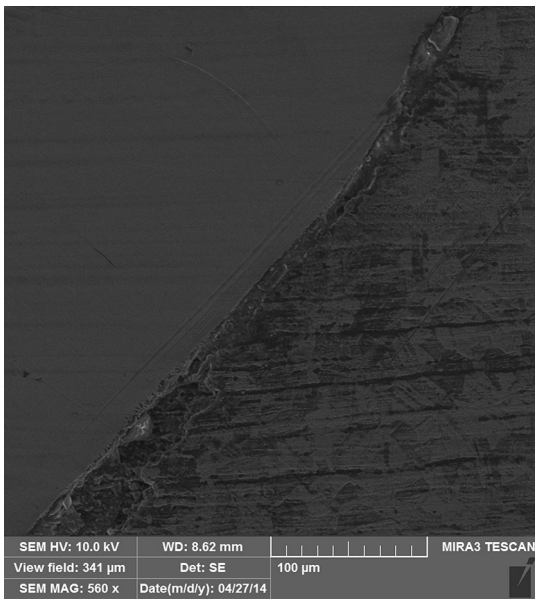

Fig. 6 Keyhole profile in Inconel 625

The energy balance equation reflects the effects of all mechanisms (first Fresnel, Multiple reflections and plasma absorption), but the effect of multiple reflection is assumed to be acting only in the horizontal direction since the angle between the multiple reflected ray and keyhole wall is assumed to be always 90° (Figs. 5, 6). Since this is not the typical case in the multiple reflections, the absorbed intensity of multiple reflections will add to the direct Fresnel intensity to produce the total absorbed intensity in the particular layer where the plasma plume absorption helps in the development of keyhole [20–24].

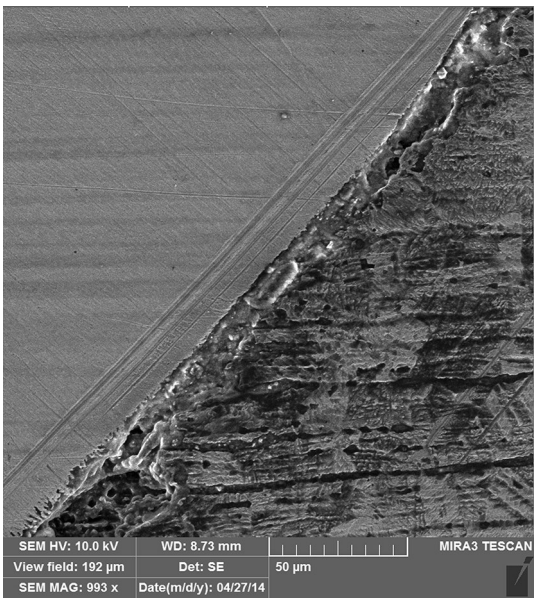

Fig. 7 Microstructure of Inconel 625 in the HAZ area

4.4 Defining of body heat flux distribution

In the number of papers published recent years, more attention was paid to the numerical models of heat sources in the laser heating process. The papers mostly utilize surface heat source models, but there are much less studies focused on the numerical models in laser beam heat sources that refers to the volumetric heat source. The laser beam heat source intensity is an exponential function that changes along the penetration depth of welded element. In this research, we used the modified version of the Goldak's volumetric heat source model [25] that is usually used for numerical modeling of the electric arc heat source power distribution. It can predict the laser power observation on the parts. So we have an optimized model for heat source power density distribution in the laser welding. A Gidak's double elliptical model for laser power density distribution is modified as follows:

$$q_{\mathrm{f}}(x,y,z) = \frac{6\sqrt{3}f_{\mathrm{f}}p_{\mathrm{abs}}}{abc_{\mathrm{f}}\pi\sqrt{\pi}} e^{\left(-3x^2/a^2\right)} e^{\left(-3x^2/b^2\right)} e^{\left(-3z^2/c_{\mathrm{f}}^2\right)} \quad (9)$$

$$q_{\mathrm{r}}(x,y,z) = \frac{6\sqrt{3}f_{\mathrm{r}}p_{\mathrm{abs}}}{abc_{\mathrm{r}}\pi\sqrt{\pi}} e^{\left(-3x^2/a^2\right)} e^{\left(-3x^2/b^2\right)} e^{\left(-3z^2/c_{\mathrm{r}}^2\right)}, \quad (10)$$

where a, b, c_{r} and c_{f}, are set of axes that define front ellipsoid and rear ellipsoid, f_{f} and f_{r} ($f_{\mathrm{r}} + f_{\mathrm{r}} = 2$) represent distribution of the heat source energy at the front and the rear section, therefore resultant distribution of the energy source is wholly described as:

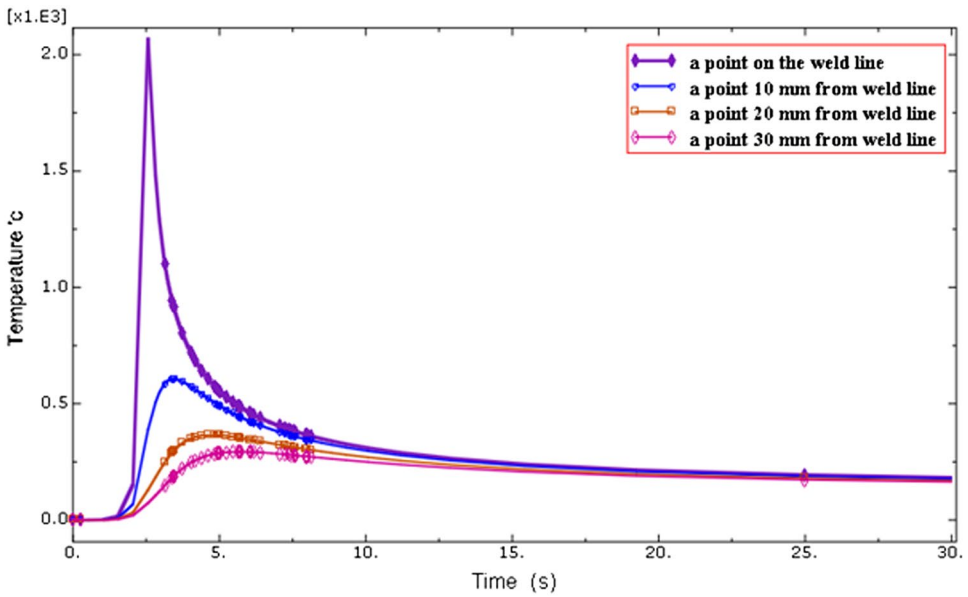

Fig. 8 Thermal history at different points in the stainless steel 304L with the laser power 500 W

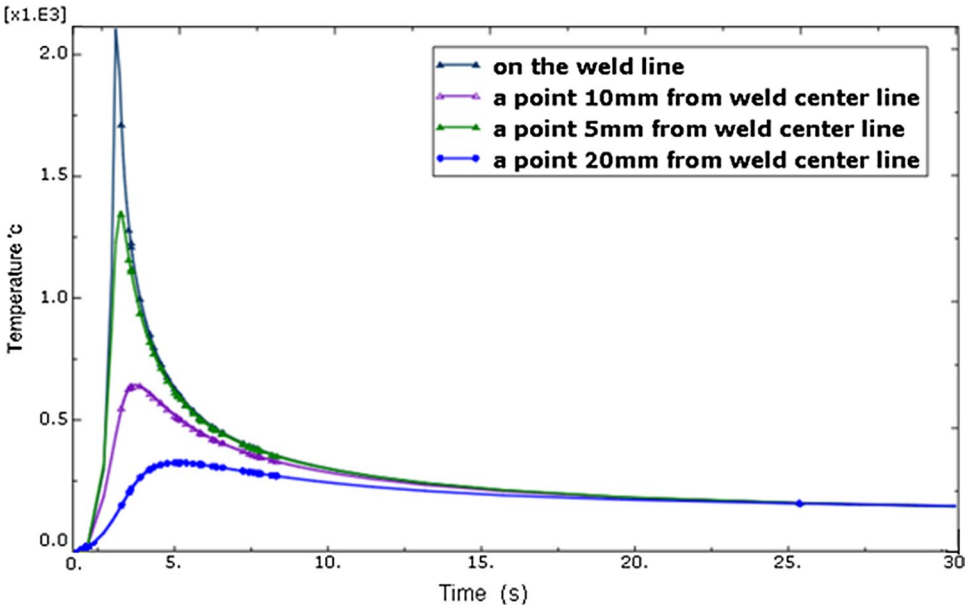

Fig. 9 Thermal history at different points in the Inconel 625 with the laser power 500 W

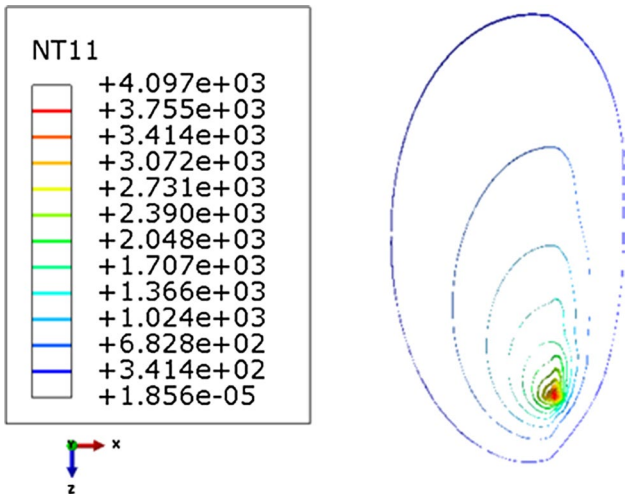

Fig. 10 Isothermal surface in laser welding of two different materials stainless steel and Inconel 628

$$q_{\text{total}}(x, y, z) = q_{\text{f}}(x, y, z) + q_{\text{r}}(x, y, z), \tag{11}$$

where p_{abs} is the absorbed laser power that is calculated in this paper [24]. In this paper to simulate butt welding of two different materials, the heat flux distribution defined in the Eq. (11) was applied.

5 Conclusion

By comparing the results of simulation and experimental results (Figs. 3, 4), we can conclude that the presented finite element model in this paper can predict the temperature distribution with little error around the different regions of the laser welded parts with different base metals. According to Figs. 8 and 9, provided the temperature history at several different points, the plots provided that the heat-affected zone is very narrow in laser beam welding. Although the extent of this region has a significant influence on the deformation and microstructure changing of welded components, laser welding can be one of the common methods for welding of very thin parts or materials that have a strong tendency to distort and microstructure change like Inconel 625. By comparing the final microstructure and thermal history diagrams, it is clear that only a very narrow region can reach the phase change temperature (Fig. 7); due to this issue, it can be argued that the presented model in this paper with high performance can predict the thermal gradient that leads to microstructure changes and deformation. By comparing the isothermal surface on each material shown in Fig. 10, it is clear that thermal distribution is unique for each material, we know that the cooling of the metal close to the weld pool is the critical metallurgical location. The results of the thermal history in this paper can be used to determine the final microstructure of laser welded part, since the absorption coefficient of laser power and reflection coefficient changes by varying the laser power. Therefore, the model presented in this paper with high precision can predict the thermal gradients.

References

1. Lingenfelter A (1989) Welding of Inconel alloy 718: a historical overview. In: Loria EA (ed) Superalloy 718: metallurgy and applications. The Minerals, Metals and Materials Society, pp 673–683
2. Radavich JF (1989) The physical metallurgy of cast and wrought alloy 718 In: Lopia EA (ed) Superalloy 718: metallurgy and

applications. The Minerals, Metals and Materials Society, pp 229–240
3. Salonitis K, Drougas D (2010) Chryssolouris G, finite element modeling of penetration laser welding of sandwich materials. J Phys Procedia 5:327–335
4. Tan W, Bailey NS, Shin YC (2013) Investigation of keyhole plume and molten pool based on a three-dimensional dynamic model with sharp interface formulation. J Phys D Appl Phys 46:055501
5. Pang S, Chen L, Zhou J, Yin Y, Chen T (2011) A three-dimensional sharp interface model for self-consistent keyhole and weld pool dynamics in deep penetration laser welding. J Phys D Appl Phys 4(4):025301
6. Vänskä M, Abt F, Weber R, Salminena A, Graf T (2013) Effects of welding parameters on to keyhole geometry for partial penetration laser welding. J. Phys Procedia 41:199–208
7. Naffakh H, Shamanian M, Ashrafizadeh F (2009) Dissimilar welding of AISI 310 austenitic stainless steel to nickel-based alloy Inconel 657. J Mater Process Technol 209:3628–3639
8. Baghjari SH, AkbariMousavi SAA (2014) Experimental investigation on dissimilar pulsed Nd:YAG laser welding of AISI 420 stainless steel to kovar alloy. J Mater Des 57:128–134
9. Al-Kazzaz H, Medraj M, Cao X, Jahazi M (2008) Nd:YAG, laser welding of aerospace grade ZE41A magnesium alloy Modeling and experimental investigations. J. Mater Chem Phys 109:61–76
10. Zhang YM, Liu YC (2007) Control of dynamic keyhole welding process. J Autom 43:876–884
11. Fujinaga S, Takenaka H, Narikiyo T, Katayama S, Matsunawa A (2000) Direct observation of keyhole behavior during pulse modulated high-power Nd:YAG laser irradiation. J Phys D Appl Phys 33:492–497
12. Volpp J, Vollertsen F (2013) Analytical modeling of the keyhole including multiple reflections for analysis of the influence of different laser intensity distributions on keyhole geometry. J. Phys Procedia 41:453–461
13. Ramkumar KD, Patel SD, Parveen SS, Choudhury DJ, Prabaharan P, Arivazhagan N, Anthony Xavior M (2014) Influence of filler metals and welding techniques on the structure property relationships of Inconel 718 and AISI 316L dissimilar weldments. J Mater Des. doi:10.1016/j.matdes.2014.05.019
14. Kaplan A (1994) A model of deep penetration laser welding based on calculation of the keyhole profile. J Phys D Appl Phys 27:1805–1814
15. Dowden J, Kapadia P, Postacioglu N (1989) An analysis of the laser-plasma interaction in laser keyhole welding. J Phys D Appl Phys 22(6):741–749
16. Solana P, Negro G (1997) A study of the effect of multiple reflections on the shape of the keyhole of the keyhole in the laser processing of materials. J Phys D Appl Phys 30:3216–3222
17. Bachmann M, Avilov V, Gumenyuk A, Rethmeier M (2014) Experimental and numerical investigation of an electromagnetic weld pool control for laser beam welding. J. Phys Procedia 56:515–524
18. Jin X, Berger P, Graf T (2006) Multiple reflections and Fresnel absorption in an actual 3D keyhole during deep penetration laser welding. J Phys D Appl Phys 39(21):4703–4712
19. Jin X, Li L, Zhang Y (2002) A study on Fresnel absorption and reflections in the keyhole in deep penetration laser welding. J Phys D Appl Phys 35:2304–2310
20. Punkari A, Weckman DC, Kerr HW (2003) Effects of magnesium content on dual beam Nd:YAG laser welding of Al–Mg alloys. J Sci Technol Weld Join 8(4):269–281
21. Lampa C, Kaplan AF, Powell J, Magnusson C (1997) An analytical thermodynamic model of laser welding. J Phys D Appl Phys 30(9):1293–1299
22. Al-Kazzaz H, Medraj M, Cao X, Xiao M, Jahazi M (2006) Effect of laser power and joint gap on weld quality of aerospace grade ZE41A-T5 magnesium alloy using Nd:YAG laser. In: Proceedings of the international symposium on magnesium, J Technology in the Global Age, p 503–518
23. Dausinger F, Rapp J, Beck M, Faisst F, Hack R, Hugel H (1996) Welding of aluminum: a challenging opportunity for laser technology. J Laser Appl 8(6):285–290
24. Swift-Hook DT, Gick AEF (1973) Penetration welding with lasers. J. Weld 52(11):492–499